Axino dark matter and baryon number asymmetry from Q-ball decay in gauge mediation

Shinta Kasuya[a], Etsuko Kawakami[b] and Masahiro Kawasaki[b,c]

[a] Department of Information Sciences, Kanagawa University, Kanagawa 259-1293, Japan
[b] Institute for Cosmic Ray Research, University of Tokyo, Chiba 277-8582, Japan
[c] Institute for the Physics and Mathematics of the Universe, University of Tokyo, Chiba 277-8582, Japan

February 18, 2012

Abstract

We investigate the Q-ball decay into the axino dark matter in the gauge-mediated supersymmetry breaking. In our scenario, the Q ball decays mainly into nucleons and partially into axinos to account for the baryon asymmetry and the dark matter of the universe simultaneously. The Q ball decays well before the big bang nucleosynthesis so that it is not affected by the decay. The decay into the supersymmetric particles of the minimal supersymmetric standard model is kinematically prohibited until the very end of the decay, and we could safely make their abundances small enough for the successful big bang nucleosynthesis. We show the regions of axino model parameters and the Q-ball parameters which realize this scenario.

1 Introduction

The origin of baryon number asymmetry and the dark matter of the universe have been discussed for decades, but are still main unsolved mysteries in cosmology. No solution can be found in the standard model (SM), and we must seek for something beyond SM. One good way is to consider supersymmetry (SUSY). In SUSY, the lightest supersymmetric particle (LSP) is, with R parity conservation, very stable and, in most cases, scarcely interacts with other particles. These natures make the LSP a strong candidate of the dark matter. SUSY could not only give a candidate of the dark matter, but also explain the origin of baryon number asymmetry. The Affleck Dine (AD) baryogenesis is one of the promising mechanism [1]. The AD field, carrying the baryon number, has a large VEV during inflation and rotates in the potential after inflation, and the baryon number is created. It finally decays into quarks to become the baryon asymmetry of the universe. In the minimal supersymmetric standard model (MSSM), there exist many flat directions, which consist of squarks, sleptons and higgs, thus carry the baryon number. Therefore, the flat direction could be responsible for the AD field.

The very attractive feature of the AD mechanism is to provide both the baryon asymmetry and the dark matter of the universe simultaneously in the context of the Q-ball cosmology [2–12]. During the rotation, the AD condensate may fragment into nontopological solitons, Q balls. These Q balls can be the dark matter if they are stable, while the LSP dark matter could be produced from unstable Q balls. Stable Q balls form if the charge Q is large enough in the gauge-mediated SUSY breaking [2, 6]. On the other hand, Q balls are unstable in the gravity mediation producing the neutralino LSP [3, 7], the gravitino LSP [8], and the axino LSP [9], and in the gauge mediation creating the gravitino LSP if the charge is small enough [10–12].

In this paper, we investigate a model where the Q ball decays into axino LSPs in gauge-mediated SUSY breaking. (Similar situation in the gravity mediation was investigated in Ref. [9].) The axino is a fermionic superpartner of the axion, which is introduced as a dynamical scalar field to solve the

strong CP problem in quantum chromodynamics known as Peccei-Quinn (PQ) mechanism [13]. In our model, Q ball decays mainly into nucleons and partially into axinos directly in order to account for both the baryon asymmetry and the dark matter of the universe. The decay of the Q ball takes place well before the big bang nucleosynthesis (BBN) so that the decay itself does not affect the BBN. Almost throughout the process, it is kinematically prohibited to decay into the lightest supersymmetric particle (LSP) of MSSM, whose decay may destroy light elements synthesized during the BBN. However, the MSSM LSPs (MLSPs) would be produced at the very end of the Q-ball decay when the charge becomes small enough to open the kinematically allowed channel to the MLSP production [14, 12]. This restricts some parameter space of the axino models. Q balls may decay into gravitinos in our scenario [12]. However, the branching into the gravitino is much smaller than that of the axino because of the much stronger coupling to the axinos than to the gravitino, and we may well neglect the contribution of the gravitino abundance to the dark matter density. Also notice that we assume the axion density is negligible in our scenario. This is simply achieved by setting the misalignment angle small enough.

The structures of this article are as follows. After briefly reviewing the Q-ball features in the gauge mediation in the next section, we show the details of the decay process of the Q ball in Sec.3. In Sec.4, we obtain the baryon and the axino dark matter abundances as well as the MLSP abundance. In Sec.5, we examine the constraints on the MLSP abundance by the BBN to derive the parameters of the axion models which lead to the successful scenario. We also show the realization of those successful scenario in the Q-ball parameters in that section. Finally, we summarize our results in Sec.6. Appendix is devoted to some details of the axino productions in the SUSY axion models which are used in the main text.

2 Q ball in gauge mediation

The AD field Φ is a combination of squarks, sleptons and higgs whose potential is flat in the SUSY exact limit. Because of the SUSY breaking in gauge mediation, the flat potential is lifted such that $V \sim m_\phi^2 \phi^2$ below the messenger scale, while it is flat above the messenger scale, $V \sim M_F^4$ [15, 2]. Here m_ϕ is a soft SUSY breaking mass and M_F is related to the F component of a gauge-singlet chiral multiplet S in the messenger sector as $M_F^4 \equiv \frac{g^2}{(4\pi)^4}\langle F_S\rangle^2$ where g is a gauge coupling constant in the standard model, and M_F is allowed in the following range:

$$10^3 \text{ GeV} \lesssim M_F \lesssim \frac{g^{1/2}}{4\pi}\sqrt{m_{3/2} M_{\rm P}}, \tag{1}$$

where $m_{3/2}$ and $M_{\rm P} = 2.4 \times 10^{18}$ GeV are the gravitino and the reduced Planck masses, respectively.

When the Hubble parameter becomes smaller than the curvature of the potential, the AD field begins to oscillate giving the baryon number. During the helical motion, it transforms into Q balls. The typical charge of the formed Q ball is estimated as [4]

$$Q = \beta \left(\frac{\phi_{\rm osc}}{M_F}\right)^4, \tag{2}$$

where $\phi_{\rm osc}$ is the field amplitude when the oscillation begins, and $\beta \simeq 6 \times 10^{-4}$ when the oscillating field has a nearly circular orbit $\epsilon = 1$ (ϵ: ellipticity of the orbit) and $\beta \simeq 6 \times 10^{-5}$ when $\epsilon \lesssim 0.1$. The charge Q is just the Φ-number, and relates to the baryon number of the Q ball as

$$B = bQ, \tag{3}$$

where b is the baryon number carried by a Φ particle. For example, $b = \frac{1}{3}$ for the udd direction. The mass, the size, the rotation velocity and the field value at the center of the Q ball are related to the

charge Q as

$$M_Q \simeq \frac{4\sqrt{2}\pi}{3} M_F Q^{3/4}, \tag{4}$$

$$R_Q \simeq \frac{1}{\sqrt{2}} M_F^{-1} Q^{1/4}, \tag{5}$$

$$\omega_Q \simeq \sqrt{2}\pi M_F Q^{-1/4}, \tag{6}$$

$$\phi_Q \simeq M_F Q^{1/4}, \tag{7}$$

respectively.

3 Q-ball decay

A Q-ball decay occurs when some decay particles have the same kind of charges as the Q ball and the mass of each decay particle is less than the Q-ball mass per charge M_Q/Q. The decay rate Γ_Q has an upper bound $\Gamma_Q^{(\mathrm{sat})}$[16]:

$$\Gamma_Q \lesssim \Gamma_Q^{(\mathrm{sat})} \simeq \frac{1}{Q} \frac{\omega_Q^3}{192\pi^2} 4\pi R_Q^2 \simeq \frac{\pi}{24\sqrt{2}} M_F Q^{-5/4}. \tag{8}$$

This saturation occurs approximately when $f_{\mathrm{eff}}\phi_Q \gtrsim \omega_Q$, where f_{eff} is the effective coupling constant by which the interaction is written as $\mathcal{L}_{\mathrm{int}} = f_{\mathrm{eff}}\phi\psi\bar{\psi}$. On the other hand, for the weak coupling limit such as $f_{\mathrm{eff}}\phi_Q \ll \omega_Q$, the decay rate is calculated as [16]

$$\Gamma_Q \simeq 3\pi \frac{f_{\mathrm{eff}}\phi_Q}{\omega_Q} \frac{1}{Q} \frac{\omega_Q^3}{192\pi^2} 4\pi R_Q^2 \simeq 3\pi \frac{f_{\mathrm{eff}}\phi_Q}{\omega_Q} \Gamma_Q^{(\mathrm{sat})}. \tag{9}$$

Here we are interested in the case where the Q ball decays into nucleons but not into MLSPs. It is described by the condition $bm_{\mathrm{N}} < M_Q/Q < m_{\mathrm{MLSP}}$ where m_N and m_{MLSP} are the nucleon and MLSP masses, respectively. This implies that the Q-ball charge should be $Q_{\mathrm{cr}} < Q < Q_{\mathrm{D}}$ where

$$Q_{\mathrm{cr}} = \frac{1024\pi^2}{81} \left(\frac{M_F}{m_{\mathrm{MLSP}}} \right)^4, \tag{10}$$

$$Q_{\mathrm{D}} = \frac{1024\pi^2}{81} \left(\frac{M_F}{bm_N} \right)^4. \tag{11}$$

The elementary process of the Q-ball decay into nucleon is squark + squark $\to$ quark + quark via gluino exchanges and the rate of this process is given by [17]

$$\Gamma(\phi\phi \to qq) \simeq \langle \sigma v \rangle \, n_\phi \simeq \frac{\zeta \alpha_s^2}{m_{\tilde{g}} \omega_Q} \omega_Q \phi_Q^2 \simeq \frac{1}{8\pi} \frac{\zeta g_s^4}{2\pi} \frac{\phi_Q^2}{m_{\tilde{g}}}, \tag{12}$$

where $m_{\tilde{g}}$ is the gluino mass, and $\zeta \sim |V_{\mathrm{CKM}}|^4$ is a possible CKM suppression factor ($10^{-3} \lesssim |V_{\mathrm{CKM}}| \lesssim 1$ [18]). Thus, the effective coupling constant f_{eff} ($\Gamma_\phi = \frac{1}{8\pi} f_{\mathrm{eff}}^2 m_\phi$) is evaluated as

$$f_{\mathrm{eff}} \simeq \frac{\zeta^{1/2} g_s^2}{\sqrt{2\pi}} \frac{\phi_Q}{(m_{\tilde{g}} \omega_Q)^{1/2}}, \tag{13}$$

where we suppose $m_\phi \simeq \omega_Q$. Since we have

$$\frac{f_{\mathrm{eff}}\phi_Q}{\omega_Q} \simeq 3.2 \times 10^{17} \zeta^{1/2} g_s^2 \left(\frac{m_{\tilde{\mathrm{g}}}}{\mathrm{TeV}} \right)^{-1/2} \left(\frac{M_F}{10^4\,\mathrm{GeV}} \right)^{1/2} \left(\frac{Q}{10^{21}} \right)^{7/8} \gg 1, \tag{14}$$

we can see that this process is saturated and the decay rate of the Q ball is given by Eq.(8). Therefore, Q balls decay at the cosmic time $t \simeq 1/\Gamma_Q^{(\rm sat)}$ when the universe is radiation-dominated, and the cosmic temperature at the decay is estimated as

$$T_{\rm D} \simeq \left(\frac{90}{4\pi^2 g_*}\right)^{1/4} \sqrt{\Gamma_Q^{(\rm sat)} M_{\rm P}} \simeq 4.3\,{\rm MeV} \left(\frac{M_F}{10^4\,{\rm GeV}}\right)^{1/2} \left(\frac{Q}{10^{21}}\right)^{-5/8}, \tag{15}$$

where g_* is the relativistic degrees of freedom at the $T_{\rm D}$ and now set to be 10.75.

Next, we consider the Q-ball decay into axinos. The condition for the decay into axinos is described by $m_{\tilde{a}} < \frac{M_Q}{Q}$. Using Eq.(4), this condition is rewritten as

$$m_{\tilde{a}} < 0.33\,{\rm GeV} \left(\frac{M_F}{10^4\,{\rm GeV}}\right) \left(\frac{Q}{10^{21}}\right)^{-1/4}. \tag{16}$$

The elementary process is squark $\to$ quark + axino whose effective coupling is given by [19]

$$f_{\rm eff}^{(\tilde{a})} = \frac{\alpha_s^2}{\sqrt{2}\pi^2} \frac{m_{\tilde{g}}}{f_a} \log\left(\frac{f_a}{m_{\tilde{g}}}\right), \tag{17}$$

which leads to

$$\frac{f_{\rm eff}^{(\tilde{a})} \phi_Q}{\omega_Q} \simeq 5.1 \times 10^{-5} \left(\frac{f_a}{10^{14}\,{\rm GeV}}\right)^{-1} \log\left(\frac{f_a}{10^3\,{\rm GeV}}\right) \left(\frac{Q}{10^{21}}\right)^{1/2}, \tag{18}$$

where f_a is the axion decay constant [1] , and we take the coupling strength for strong interaction as $\alpha_s = 0.1$ and the gluino mass $m_{\tilde{g}} = 1\,{\rm TeV}$. The decay may be saturated depending on the parameters f_a and Q, contrary to the case of the gravitino dark matter [12]. If the decay is not saturated, the branching ratio of the decay into the axinos can be calculated as

$$B_{\tilde{a}} \equiv \frac{\Gamma_Q^{(\tilde{a})}}{\Gamma_Q^{(\rm sat)}} \simeq 3\pi \frac{f_{\rm eff}^{(\tilde{a})} \phi_Q}{\omega_Q} \simeq 4.8 \times 10^{-4} \left(\frac{f_a}{10^{14}\,{\rm GeV}}\right)^{-1} \log\left(\frac{f_a}{10^3\,{\rm GeV}}\right) \left(\frac{Q}{10^{21}}\right)^{1/2}, \tag{19}$$

while $B_{\tilde{a}} = O(1)$ when the decay saturates. In the latter case, we set $B_{\tilde{a}} = 1$ below for simplicity.

One may wonder if the gravitinos are abundantly produced by the Q-ball decay in this senario. To examine this, we estimate the ratio $B_{\tilde{a}}/B_{3/2}$:

$$\frac{B_{\tilde{a}}}{B_{3/2}} \simeq \begin{cases} \dfrac{1}{B_{3/2}} \simeq 1.4 \times 10^9 \left(\dfrac{M_F}{10^4\,{\rm GeV}}\right)^{-2} \left(\dfrac{m_{3/2}}{\rm GeV}\right) & \text{(for the saturated case),} \\ \dfrac{f_{\rm eff}^{(\tilde{a})}}{f_{\rm eff}^{(3/2)}} \simeq 6.7 \times 10^5 \left(\dfrac{f_a}{10^{14}\,{\rm GeV}}\right)^{-1} \log\left(\dfrac{f_a}{10^3\,{\rm GeV}}\right) & \\ \qquad \times \left(\dfrac{M_F}{10^4\,{\rm GeV}}\right)^{-2} \left(\dfrac{Q}{10^{21}}\right)^{1/2} \left(\dfrac{m_{3/2}}{\rm GeV}\right) & \text{(for the unsaturated case).} \end{cases} \tag{20}$$

Here we use $f_{\rm eff}^{(3/2)} \simeq \frac{1}{\sqrt{6}} \frac{\omega_Q^2}{m_{3/2} M_{\rm P}}$ [12]. Therefore, there is essentially no gravitino production in the decay of the Q ball for the parameters which we find for the successful scenario in this paper.

[1] We regard f_a as $f_a/N_{\rm c}$ throughout the paper, where $N_{\rm c}$ is the color anomaly of the PQ symmetry.

4 Baryon, axino and MLSP abundances from Q-ball decay

In this section, we estimate the number densities of the baryon and the axino dark matter. We also calculate the MLSP abundance which is constrained by the BBN observation and by the upper limit of the reheating temperature which comes from the requirement that the thermally produced axinos and/or gravitinos should not be the main component of the dark matter of the universe. The analysis largely follows Ref. [12].

The number densities of the baryon, the axino and the MLSP are expressed in terms of the AD field number density n_ϕ as

$$n_b \simeq \epsilon b n_\phi, \tag{21}$$

$$n_{\tilde{a}} \simeq B_{\tilde{a}} n_\phi, \tag{22}$$

$$n_{\rm MLSP} \simeq \frac{Q_{\rm cr}}{Q} n_\phi, \tag{23}$$

respectively, where $B_{\tilde{a}} = 1$ in the saturated case. From the observations (such as the WMAP observation [20]), the ratio of the dark matter to baryon energy densities is $\rho_{\rm DM}/\rho_b \simeq 5$, so

$$\frac{\rho_{\tilde{a}}}{\rho_b} \simeq \frac{m_{\tilde{a}} B_{\tilde{a}}}{m_N \epsilon b} \simeq 5. \tag{24}$$

This gives an expression for ϵ such that

$$\epsilon \simeq \frac{m_{\tilde{a}}}{m_N}\frac{B_{\tilde{a}}}{5b} \simeq \frac{9.6\times 10^{-5}}{b}\left(\frac{m_{\tilde{a}}}{\rm GeV}\right)\left(\frac{f_a}{10^{14}\,{\rm GeV}}\right)^{-1}\log\left(\frac{f_a}{10^3\,{\rm GeV}}\right)\left(\frac{Q}{10^{21}}\right)^{1/2}. \tag{25}$$

Therefore, the orbit of the AD field is typically oblate, and we generally set $\beta = 6\times 10^{-5}$ below. The baryon number is estimated as [12]

$$Y_b \equiv \frac{n_b}{s} \simeq \frac{9}{8\sqrt{2}}\epsilon b \beta^{-3/4}\frac{M_F T_{\rm RH}}{M_{\rm P}^2}Q^{3/4} \simeq \frac{9}{8\sqrt{2}}\frac{m_{\tilde{a}} B_{\tilde{a}}}{5 m_N}\beta^{-3/4}\frac{M_F T_{\rm RH}}{M_{\rm P}^2}Q^{3/4}, \tag{26}$$

where we used Eq.(24) in the second equality. For the saturated case, that is, $B_{\tilde{a}} = 1$, Y_b is obtained as

$$\left.\frac{Y_b}{10^{-10}}\right|_{\rm sat} \simeq 2.3\times 10^2\left(\frac{m_{\tilde{a}}}{\rm GeV}\right)\left(\frac{\beta}{6\times 10^{-5}}\right)^{-3/4}\left(\frac{T_{\rm RH}}{10^7\,{\rm GeV}}\right)\left(\frac{M_F}{10^4\,{\rm GeV}}\right)\left(\frac{Q}{10^{21}}\right)^{3/4}, \tag{27}$$

and, for the unsaturated case, Y_b becomes

$$\begin{aligned}\left.\frac{Y_b}{10^{-10}}\right|_{\rm unsat} \simeq\ & 0.11\left(\frac{m_{\tilde{a}}}{\rm GeV}\right)\left(\frac{f_a}{10^{14}\,{\rm GeV}}\right)^{-1}\log\left(\frac{f_a}{10^3\,{\rm GeV}}\right)\left(\frac{\beta}{6\times 10^{-5}}\right)^{-3/4} \\ & \times\left(\frac{T_{\rm RH}}{10^7\,{\rm GeV}}\right)\left(\frac{M_F}{10^4\,{\rm GeV}}\right)\left(\frac{Q}{10^{21}}\right)^{5/4}.\end{aligned} \tag{28}$$

From these equations, we get relations among the parameters assuming $Y_b = 10^{-10}$.

On the other hand, the MLSP abundance is estimated as

$$\begin{aligned}\frac{\rho_{\rm MLSP}}{s} &= m_{\tilde{a}} Y_{\tilde{a}} \frac{\rho_{\rm MLSP}}{\rho_{\tilde{a}}} \\ &\simeq 5 m_N Y_b \frac{m_{\rm MLSP} n_{\rm MLSP}}{m_{\tilde{a}} n_{\tilde{a}}} \\ &\simeq 5 m_N Y_b \frac{m_{\rm MLSP}}{m_{\tilde{a}}}\frac{1024\pi^4}{81}\left(\frac{M_F}{m_{\rm MLSP}}\right)^4 \frac{n_\phi}{Q}\frac{1}{B_{\tilde{a}} n_\phi}.\end{aligned} \tag{29}$$

In the saturated case, this becomes,

$$\frac{\rho_{\rm MLSP}}{s}\Big|_{\rm sat} \simeq 6.2\times10^{-18}\,{\rm GeV}\left(\frac{Y_b}{10^{-10}}\right)\left(\frac{m_{\tilde a}}{\rm GeV}\right)^{-1}\left(\frac{m_{\rm MLSP}}{100\,{\rm GeV}}\right)^{-3}\left(\frac{M_F}{10^4\,{\rm GeV}}\right)^4\left(\frac{Q}{10^{21}}\right)^{-1}, \quad (30)$$

and, in the unsaturated case, we have

$$\frac{\rho_{\rm MLSP}}{s}\Big|_{\rm unsat} \simeq 1.3\times10^{-14}\,{\rm GeV}\left(\frac{Y_b}{10^{-10}}\right)\left(\frac{m_{\tilde a}}{\rm GeV}\right)^{-1}\left(\frac{f_a}{10^{14}\,{\rm GeV}}\right)\left(\log\frac{f_a}{10^3\,{\rm GeV}}\right)^{-1}\left(\frac{m_{\rm MLSP}}{100\,{\rm GeV}}\right)^{-3} \times\left(\frac{M_F}{10^4\,{\rm GeV}}\right)^4\left(\frac{Q}{10^{21}}\right)^{-3/2}. \quad (31)$$

5 Constraints on models

In this section, we see that the MLSP abundance is bounded from above by BBN constraints in Sec. 5.1, and, in Sec. 5.2, bounded from below by the highest possible reheating temperature such that thermally produced axinos or gravitinos do not dominate the dark matter in the universe. We show the allowed region for the axino parameters f_a and $m_{\tilde a}$ in Sec. 5.3, and, for the Q-ball parameters Q and M_F in Sec. 5.4.

5.1 BBN constraints on the MLSP abundance

The upper limit on the MLSP abundance is given by the fact that the decay of the MLSP may affect abundances of light elements synthesized during the BBN. The constraints can be estimated approximately as [21]

$$\frac{\rho_{\rm MLSP}}{s} \lesssim \begin{cases} 10^{-10}\,{\rm GeV}\left(\frac{m_{\rm MLSP}}{100\,{\rm GeV}}\right)^{0.6} & (1\,{\rm sec}\lesssim\tau_{\rm MLSP}\lesssim100\,{\rm sec}), \\ 4\times10^{-14}\,{\rm GeV}\left(\frac{m_{\rm MLSP}}{100\,{\rm GeV}}\right)^{0.4} & (100\,{\rm sec}\lesssim\tau_{\rm MLSP}\lesssim10^7\,{\rm sec}), \\ 10^{-14}\,{\rm GeV} & (10^7\,{\rm sec}\lesssim\tau_{\rm MLSP}), \end{cases} \quad (32)$$

where $\tau_{\rm MLSP}$ is the life time of the MLSP. From the decay rate of the neutralino into the axino Eq.(A.12), the lifetime is calculated as

$$\tau_{\rm MLSP} = 4.9\times10^5\ {\rm sec}\left(\frac{f_a}{10^{14}\,{\rm GeV}}\right)^2\left(\frac{m_{\rm MLSP}}{100\,{\rm GeV}}\right)^{-3}. \quad (33)$$

Therefore, we obtain the upper bound of the MLSP abundance as[2]

$$\frac{\rho_{\rm MLSP}}{s} \lesssim \begin{cases} 10^{-10}\,{\rm GeV}\left(\frac{m_{\rm MLSP}}{100\,{\rm GeV}}\right)^{0.6} & \left(1\times10^{11}\,{\rm GeV}\lesssim\tilde f_a\lesssim1\times10^{12}\,{\rm GeV}\right), \\ 4\times10^{-14}\,{\rm GeV}\left(\frac{m_{\rm MLSP}}{100\,{\rm GeV}}\right)^{0.4} & \left(1\times10^{12}\,{\rm GeV}\lesssim\tilde f_a\lesssim5\times10^{14}\,{\rm GeV}\right), \\ 10^{-14}\,{\rm GeV} & \left(5\times10^{14}\,{\rm GeV}\lesssim\tilde f_a\right), \end{cases} \quad (34)$$

where $\tilde f_a = f_a\left(\frac{m_{\rm MLSP}}{100\,{\rm GeV}}\right)^{-3/2}$. This is shown in blue solid lines in Fig. 1.

[2] The range of f_a slightly differs for the stau MLSP.

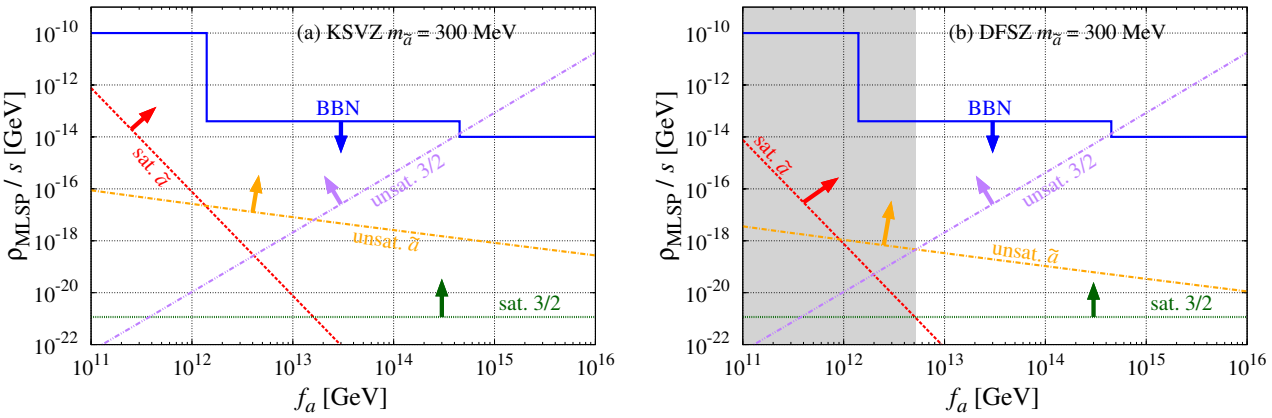

Figure 1: Constraints on the MLSP abundance for $m_{\rm MLSP} = 100$ GeV in (a) the KSVZ and (b) the DFSZ models with $m_{\tilde{a}} = 300\,\text{MeV}$. In both panels, the BBN constraint [Eq.(34)] is denoted as the blue solid lines. Red dashed and green dotted lines represent the lower limits in the saturated Q-ball decay with the highest possible reheating temperature determined by thermally produced axinos and gravitinos, respectively [Eqs.(40) and (45) for the KSVZ and DFSZ models, respectively]. On the other hand, orange dashed dotted and purple dashed double-dotted lines show the lower bounds in the unsaturated Q-ball decay with the highest possible reheating temperature determined by thermally produced axinos and gravitinos, respectively [Eqs.(41) and (46) for the KSVZ and DFSZ models, respectively]. The gray region in the right panel (b) is excluded by the overabundance of the axinos from the higgsino decay [Eq.(44)].

5.2 Lowest possible abundance of the MLSP

The lower limit on the MLSP abundance comes from constraints on the reheating temperature. The constraints are due to the condition that thermally produced axinos and gravitinos cannot be the dominant component of the dark matter in the universe.

Let us first see how the MLSP abundance depends on the reheating temperature $T_{\rm RH}$. Using Eqs.(15) and (27) with $Y_b = 10^{-10}$ to eliminate Q and M_F from Eq.(30), we obtain

$$\left.\frac{\rho_{\rm MLSP}}{s}\right|_{\rm sat} \simeq 2.8\times10^{-23}\,\text{GeV}\left(\frac{m_{\tilde{a}}}{\text{GeV}}\right)^{-3}\left(\frac{\beta}{6\times10^{-5}}\right)^{3/2}\left(\frac{m_{\rm MLSP}}{100\,\text{GeV}}\right)^{-3}\left(\frac{T_{\rm RH}}{10^7\,\text{GeV}}\right)^{-2}\left(\frac{T_{\rm D}}{3\,\text{MeV}}\right)^{4}, \tag{35}$$

for the saturated case. On the other hand, using Eqs.(15) and (28) with $Y_b = 10^{-10}$ to eliminate Q and M_F from Eq.(31), we have

$$\begin{aligned}\left.\frac{\rho_{\rm MLSP}}{s}\right|_{\rm unsat} \simeq\ & 4.4\times10^{-14}\,\text{GeV}\left(\frac{m_{\tilde{a}}}{\text{GeV}}\right)^{-12/5}\left(\frac{f_a}{10^{14}\,\text{GeV}}\right)^{12/5}\left(\log\frac{f_a}{10^3\,\text{GeV}}\right)^{-12/5}\\ &\times\left(\frac{\beta}{6\times10^{-5}}\right)^{21/20}\left(\frac{m_{\rm MLSP}}{100\,\text{GeV}}\right)^{-3}\left(\frac{T_{\rm RH}}{10^7\,\text{GeV}}\right)^{-7/5}\left(\frac{T_{\rm D}}{3\,\text{MeV}}\right)^{26/5},\end{aligned} \tag{36}$$

for the unsaturated case.

The upper limit of $T_{\rm RH}$ comes from the requirement that the thermally produced axinos and gravitinos should satisfy $\max(\Omega^{\rm TH}_{\tilde{a}}h^2, \Omega^{\rm TH}_{3/2}h^2) \lesssim \Omega_{\rm DM}h^2 \simeq 0.11$, where $\Omega^{\rm TH}_{\tilde{a}}$ and $\Omega^{\rm TH}_{3/2}$ respectively denote the density parameters of thermally produced axino and gravitino, and h is the Hubble constant

in units of 100 km/s/Mpc. The constraint from the gravitino is written as [22],

$$T_{\rm RH} \lesssim T_{\rm RH,max}^{(3/2)} \equiv 3\times10^7\,{\rm GeV}\left(\frac{m_{\tilde g}}{500\,{\rm GeV}}\right)^{-2}\left(\frac{m_{3/2}}{\rm GeV}\right), \simeq 3\times10^7\,{\rm GeV}\left(\frac{m_{\tilde a}}{\rm GeV}\right), \tag{37}$$

where the gravitino mass is assumed to be the same as the axino mass $m_{\tilde a}$[3]. On the other hand, the constraint from the axino depends on axion models. Here we consider two classes of axion models, the Kim-Shifman-Vainshtein-Zakharov (KSVZ) and Dine-Fischer-Srednicki-Zhitnitskii (DFSZ) models. Some details of the axino which we use in the main text are shown in Appendix.

5.2.1 KSVZ model

In the KSVZ model, the thermally produced axino density parameter is given by [24]

$$\Omega_{\tilde a}^{\rm TH}h^2 \simeq 1.0\times10^{-2}\left(\frac{m_{\tilde a}}{\rm GeV}\right)\left(\frac{f_a}{10^{14}\,{\rm GeV}}\right)^{-2}\left(\frac{T_{\rm RH}}{10^7\,{\rm GeV}}\right). \tag{38}$$

See Eq.(A.8). From $\Omega_{\tilde a}^{\rm TH}h^2 \lesssim \Omega_{\rm DM}h^2 \simeq 0.11$, the constraint on $T_{\rm RH}$ reads as

$$T_{\rm RH} \lesssim T_{\rm RH,max}^{(\rm KSVZ\ \tilde a)} \equiv 1.1\times10^8\ {\rm GeV}\left(\frac{m_{\tilde a}}{\rm GeV}\right)^{-1}\left(\frac{f_a}{10^{14}\,{\rm GeV}}\right)^2. \tag{39}$$

Inserting this or Eq.(37) into Eqs.(35) and (36), we obtain the lowest possible abundances of the MLSP in the saturated and the unsaturated cases respectively as

$$\left.\frac{\rho_{\rm MLSP}}{s}\right|_{\rm sat} \gtrsim \begin{cases} 2.3\times10^{-25}\,{\rm GeV}\left(\frac{m_{\tilde a}}{\rm GeV}\right)^{-1}\left(\frac{f_a}{10^{14}\,{\rm GeV}}\right)^{-4}\left(\frac{\beta}{6\times10^{-5}}\right)^{3/2}\left(\frac{m_{\rm MLSP}}{100\,{\rm GeV}}\right)^{-3}\left(\frac{T_{\rm D}}{3\,{\rm MeV}}\right)^4, \\ \qquad\qquad \left(T_{\rm RH,max}^{(\rm KSVZ\ \tilde a)} < T_{\rm RH,max}^{(3/2)}\right), \\ 3.1\times10^{-24}\,{\rm GeV}\left(\frac{m_{\tilde a}}{\rm GeV}\right)^{-5}\left(\frac{\beta}{6\times10^{-5}}\right)^{3/2}\left(\frac{m_{\rm MLSP}}{100\,{\rm GeV}}\right)^{-3}\left(\frac{T_{\rm D}}{3\,{\rm MeV}}\right)^4, \\ \qquad\qquad \left(T_{\rm RH,max}^{(\rm KSVZ\ \tilde a)} > T_{\rm RH,max}^{(3/2)}\right), \end{cases} \tag{40}$$

$$\left.\frac{\rho_{\rm MLSP}}{s}\right|_{\rm unsat} \gtrsim \begin{cases} 1.5\times10^{-15}\,{\rm GeV}\left(\frac{m_{\tilde a}}{\rm GeV}\right)^{-1}\left(\frac{f_a}{10^{14}\,{\rm GeV}}\right)^{-2/5}\left(\log\frac{f_a}{10^3\,{\rm GeV}}\right)^{-12/5} \\ \qquad\times\left(\frac{\beta}{6\times10^{-5}}\right)^{21/20}\left(\frac{m_{\rm MLSP}}{100\,{\rm GeV}}\right)^{-3}\left(\frac{T_{\rm D}}{3\,{\rm MeV}}\right)^{26/5}, \\ \qquad\qquad \left(T_{\rm RH,max}^{(\rm KSVZ\ \tilde a)} < T_{\rm RH,max}^{(3/2)}\right), \\ 9.5\times10^{-15}\,{\rm GeV}\left(\frac{m_{\tilde a}}{\rm GeV}\right)^{-19/5}\left(\frac{f_a}{10^{14}\,{\rm GeV}}\right)^{12/5}\left(\log\frac{f_a}{10^3\,{\rm GeV}}\right)^{-12/5} \\ \qquad\times\left(\frac{\beta}{6\times10^{-5}}\right)^{21/20}\left(\frac{m_{\rm MLSP}}{100\,{\rm GeV}}\right)^{-3}\left(\frac{T_{\rm D}}{3\,{\rm MeV}}\right)^{26/5}, \\ \qquad\qquad \left(T_{\rm RH,max}^{(\rm KSVZ\ \tilde a)} > T_{\rm RH,max}^{(3/2)}\right). \end{cases} \tag{41}$$

These four kinds of the lower limits of the MLSP abundance are shown in the left panel of Fig. 1 for $m_{\tilde a} = 300\,{\rm MeV}$. There, the allowed region is above the uppermost among these four lines, and below the BBN constraint line Eq.(34).

[3] $m_a \simeq m_{3/2}$ is natural, although the axino mass may vary large depending on the actual models [23].

5.2.2 DFSZ model

In the DFSZ model, the axino production is dominated by the higgsino decay through the axino-Higgsino-Higgs interaction at the low reheating temperature ($T_{\rm RH} \lesssim 2\times10^7\,{\rm GeV}$) [25], while by scatterings due to $SU(2)_L$ coupling at the high reheating temperature ($T_{\rm RH} \gtrsim 2\times10^7\,{\rm GeV}$). Thus the abundance of thermally produced axinos can be estimated as [26]

$$\Omega_{\tilde a}^{\rm TH}h^2 \simeq \begin{cases} 2.0\times10^{-3}\left(\dfrac{m_{\tilde a}}{\rm GeV}\right)\left(\dfrac{f_a}{10^{14}\,{\rm GeV}}\right)^{-2} & \left(T_{\rm RH}\lesssim 2\times10^7\,{\rm GeV}\right), \\ 1.0\times10^{-3}\left(\dfrac{m_{\tilde a}}{\rm GeV}\right)\left(\dfrac{f_a}{10^{14}\,{\rm GeV}}\right)^{-2}\left(\dfrac{T_{\rm RH}}{10^7\,{\rm GeV}}\right) & \left(T_{\rm RH}\gtrsim 2\times10^7\,{\rm GeV}\right). \end{cases} \tag{42}$$

See Eqs.(A.11) and (A.9). For $T_{\rm RH} \gtrsim 2\times10^7\,{\rm GeV}$, we obtain the upper limit on $T_{\rm RH}$ as

$$T_{\rm RH} \lesssim T_{\rm RH,max}^{(\rm DFSZ\ \tilde a)} \equiv 1.1\times10^9\,{\rm GeV}\left(\frac{m_{\tilde a}}{\rm GeV}\right)^{-1}\left(\frac{f_a}{10^{14}\,{\rm GeV}}\right)^{2}. \tag{43}$$

On the other hand, for $T_{\rm RH} \lesssim 2\times10^7\,{\rm GeV}$, the condition $\Omega_{\tilde a}^{\rm TH}h^2 \lesssim \Omega_{\rm DM}h^2 \simeq 0.11$ only leads to the constraint on f_a and $m_{\tilde a}$ as

$$\left(\frac{m_{\tilde a}}{\rm GeV}\right)\left(\frac{f_a}{10^{14}\,{\rm GeV}}\right)^{-2} \lesssim 55, \tag{44}$$

and we must use $T_{\rm RH,max}^{(3/2)}$ in order to obtain the lowest possible abundance. Therefore, we have

$$\frac{\rho_{\rm MLSP}}{s}\Big|_{\rm sat} \gtrsim \begin{cases} 2.3\times10^{-27}{\rm GeV}\left(\dfrac{m_{\tilde a}}{\rm GeV}\right)^{-1}\left(\dfrac{f_a}{10^{14}\,{\rm GeV}}\right)^{-4}\left(\dfrac{\beta}{6\times10^{-5}}\right)^{3/2}\left(\dfrac{m_{\rm MLSP}}{100\,{\rm GeV}}\right)^{-3}\left(\dfrac{T_{\rm D}}{3\,{\rm MeV}}\right)^{4}, \\ \qquad\qquad \left(T_{\rm RH,max}^{(\rm DFSZ\ \tilde a)} < T_{\rm RH,max}^{(3/2)} \text{ and } T_{\rm RH}\gtrsim 2\times10^7\,{\rm GeV}\right), \\ 3.1\times10^{-24}\,{\rm GeV}\left(\dfrac{m_{\tilde a}}{\rm GeV}\right)^{-5}\left(\dfrac{\beta}{6\times10^{-5}}\right)^{3/2}\left(\dfrac{m_{\rm MLSP}}{100\,{\rm GeV}}\right)^{-3}\left(\dfrac{T_{\rm D}}{3\,{\rm MeV}}\right)^{4}, \\ \qquad\qquad \left(T_{\rm RH,max}^{(\rm DFSZ\ \tilde a)} > T_{\rm RH,max}^{(3/2)} \text{ or } T_{\rm RH}\lesssim 2\times10^7\,{\rm GeV}\right), \end{cases} \tag{45}$$

$$\frac{\rho_{\rm MLSP}}{s}\Big|_{\rm unsat} \gtrsim \begin{cases} 6.1\times10^{-17}\,{\rm GeV}\left(\dfrac{m_{\tilde a}}{\rm GeV}\right)^{-1}\left(\dfrac{f_a}{10^{14}\,{\rm GeV}}\right)^{-2/5}\left(\log\dfrac{f_a}{10^3\,{\rm GeV}}\right)^{-12/5} \\ \qquad\qquad \times\left(\dfrac{\beta}{6\times10^{-5}}\right)^{21/20}\left(\dfrac{m_{\rm MLSP}}{100\,{\rm GeV}}\right)^{-3}\left(\dfrac{T_{\rm D}}{3\,{\rm MeV}}\right)^{26/5}, \\ \qquad\qquad \left(T_{\rm RH,max}^{(\rm DFSZ\ \tilde a)} < T_{\rm RH,max}^{(3/2)} \text{ and } T_{\rm RH}\gtrsim 2\times10^7\,{\rm GeV}\right), \\ 9.5\times10^{-15}\,{\rm GeV}\left(\dfrac{m_{\tilde a}}{\rm GeV}\right)^{-19/5}\left(\dfrac{f_a}{10^{14}\,{\rm GeV}}\right)^{12/5}\left(\log\dfrac{f_a}{10^3\,{\rm GeV}}\right)^{-12/5} \\ \qquad\qquad \times\left(\dfrac{\beta}{6\times10^{-5}}\right)^{21/20}\left(\dfrac{m_{\rm MLSP}}{100\,{\rm GeV}}\right)^{-3}\left(\dfrac{T_{\rm D}}{3\,{\rm MeV}}\right)^{26/5}, \\ \qquad\qquad \left(T_{\rm RH,max}^{(\rm DFSZ\ \tilde a)} > T_{\rm RH,max}^{(3/2)} \text{ or } T_{\rm RH}\lesssim 2\times10^7\,{\rm GeV}\right). \end{cases} \tag{46}$$

These four kinds of the abundances are shown in the right panel of Fig. 1 for $m_{\tilde a}$ =300 MeV. The allowed region is above the uppermost among these four lines, and below the BBN constraint line Eq(34). Notice that the lower f_a region is excluded by the constraint Eq.(44), above which too much axinos will be produced by the higgsino decay.

5.3 Constraints on axino model parameters

Here we put constraints on the parameters $m_{\tilde{a}}$ and f_a. They are restricted by the condition that there exists the allowed range for the MLSP abundance; the lowest possible MLSP abundance, Eqs.(40) or (41) for the KSVZ model and Eqs.(45) or (46) for the DFSZ model, must be smaller than the upper limits from the BBN [Eq.(34)]. As is clear in Fig. 2 below, the lowest possible abundance of MLSPs is determined by the highest possible reheating temperature for the gravitino, $T_{\rm RH,max}^{(3/2)}$, so that the constraints are the same for both KSVZ and DFSZ models. Therefore, we obtain the following constraints on (f_a, $m_{\tilde{a}}$) plane:

$$
m_{\tilde{a}} \gtrsim \begin{cases}
2.0\times10^{-3}\,{\rm GeV}\left(\dfrac{\beta}{6\times10^{-5}}\right)^{3/10}\left(\dfrac{m_{\rm MLSP}}{100\,{\rm GeV}}\right)^{-0.72}\left(\dfrac{T_{\rm D}}{3\,{\rm MeV}}\right)^{4/5}, \\
\qquad\qquad\qquad\qquad\qquad\qquad\qquad\qquad\left(1\times10^{11}\,{\rm GeV}\lesssim\tilde{f}_a\lesssim1\times10^{12}\,{\rm GeV}\right), \\
2.4\times10^{-2}\,{\rm GeV}\left(\dfrac{\beta}{6\times10^{-5}}\right)^{3/10}\left(\dfrac{m_{\rm MLSP}}{100\,{\rm GeV}}\right)^{-0.68}\left(\dfrac{T_{\rm D}}{3\,{\rm MeV}}\right)^{4/5}, \\
\qquad\qquad\qquad\qquad\qquad\qquad\qquad\qquad\left(1\times10^{12}\,{\rm GeV}\lesssim\tilde{f}_a\lesssim3\times10^{12}\,{\rm GeV}\right), \\
0.69\,{\rm GeV}\left(\dfrac{f_a}{10^{14}\,{\rm GeV}}\right)^{12/19}\left(\log\dfrac{f_a}{10^{3}\,{\rm GeV}}\right)^{-12/19}\left(\dfrac{\beta}{6\times10^{-5}}\right)^{21/76}\left(\dfrac{m_{\rm MLSP}}{100\,{\rm GeV}}\right)^{-0.90}\left(\dfrac{T_{\rm D}}{3\,{\rm MeV}}\right)^{26/19}, \\
\qquad\qquad\qquad\qquad\qquad\qquad\qquad\qquad\left(3\times10^{12}\,{\rm GeV}\lesssim\tilde{f}_a\lesssim5\times10^{14}\,{\rm GeV}\right), \\
0.99\,{\rm GeV}\left(\dfrac{f_a}{10^{14}\,{\rm GeV}}\right)^{12/19}\left(\log\dfrac{f_a}{10^{3}\,{\rm GeV}}\right)^{-12/19}\left(\dfrac{\beta}{6\times10^{-5}}\right)^{21/76}\left(\dfrac{m_{\rm MLSP}}{100\,{\rm GeV}}\right)^{-15/19}\left(\dfrac{T_{\rm D}}{3\,{\rm MeV}}\right)^{26/19}, \\
\qquad\qquad\qquad\qquad\qquad\qquad\qquad\qquad\left(5\times10^{14}\,{\rm GeV}\lesssim\tilde{f}_a\right).
\end{cases}
\tag{47}
$$

These are shown in blue solid lines in Fig. 2.

In addition, there are other constraints on these parameters. One is that Q balls must be kinematically allowed to decay into axinos, which is expressed as Eq.(16). Rewriting it in terms of the MLSP abundance using Eq.(30), we have

$$
m_{\tilde{a},\rm sat} < 0.12\,{\rm GeV}\left(\frac{\rho_{\rm MLSP}/s}{10^{-18}\,{\rm GeV}}\right)^{1/3}\left(\frac{m_{\rm MLSP}}{100\,{\rm GeV}}\right)\left(\frac{Y_b}{10^{-10}}\right)^{-1/3}, \tag{48}
$$

for the saturated case, and

$$
\begin{aligned}
m_{\tilde{a},\rm unsat} < 0.22\,{\rm GeV}&\left(\frac{\rho_{\rm MLSP}/s}{10^{-14}\,{\rm GeV}}\right)^{2/5}\left(\frac{m_{\rm MLSP}}{100\,{\rm GeV}}\right)^{6/5}\left(\frac{Y_b}{10^{-10}}\right)^{-2/5} \\
&\times\left(\frac{f_a}{10^{14}\,{\rm GeV}}\right)^{-2/5}\left(\log\frac{f_a}{10^{3}\,{\rm GeV}}\right)^{2/5}\left(\frac{T_{\rm D}}{3\,{\rm MeV}}\right)^{-2/5},
\end{aligned}
\tag{49}
$$

for the unsaturated case using Eqs.(31) and (15). Then, inserting the upper bound of the MLSP abundance from the BBN constraints Eq.(34), we obtain the upper limit on $m_{\tilde{a}}$ such as

$$
m_{\tilde{a},\rm sat} \lesssim \begin{cases}
58\,{\rm GeV}\left(\dfrac{m_{\rm MLSP}}{100\,{\rm GeV}}\right)^{1.2}\left(\dfrac{Y_b}{10^{-10}}\right)^{-1/3} & \left(1\times10^{11}\,{\rm GeV}\lesssim\tilde{f}_a\lesssim1\times10^{12}\,{\rm GeV}\right), \\
4.3\,{\rm GeV}\left(\dfrac{m_{\rm MLSP}}{100\,{\rm GeV}}\right)^{1.13}\left(\dfrac{Y_b}{10^{-10}}\right)^{-1/3} & \left(1\times10^{12}\,{\rm GeV}\lesssim\tilde{f}_a\lesssim5\times10^{14}\,{\rm GeV}\right), \\
2.7\,{\rm GeV}\left(\dfrac{m_{\rm MLSP}}{100\,{\rm GeV}}\right)\left(\dfrac{Y_b}{10^{-10}}\right)^{-1/3} & \left(5\times10^{14}\,{\rm GeV}\lesssim\tilde{f}_a\right).
\end{cases}
\tag{50}
$$

$$
m_{\tilde{a},\mathrm{unsat}} \lesssim \begin{cases} 8.8\,\mathrm{GeV}\left(\dfrac{m_{\mathrm{MLSP}}}{100\,\mathrm{GeV}}\right)^{1.44}\left(\dfrac{Y_b}{10^{-10}}\right)^{-2/5}\left(\dfrac{f_a}{10^{14}\,\mathrm{GeV}}\right)^{-2/5}\left(\log\dfrac{f_a}{10^3\,\mathrm{GeV}}\right)^{2/5}\left(\dfrac{T_\mathrm{D}}{3\,\mathrm{MeV}}\right)^{-2/5}, \\ \qquad\qquad \left(1\times10^{11}\,\mathrm{GeV}\lesssim\tilde{f}_a\lesssim 1\times10^{12}\,\mathrm{GeV}\right), \\ 0.38\,\mathrm{GeV}\left(\dfrac{m_{\mathrm{MLSP}}}{100\,\mathrm{GeV}}\right)^{1.36}\left(\dfrac{Y_b}{10^{-10}}\right)^{-2/5}\left(\dfrac{f_a}{10^{14}\,\mathrm{GeV}}\right)^{-2/5}\left(\log\dfrac{f_a}{10^3\,\mathrm{GeV}}\right)^{2/5}\left(\dfrac{T_\mathrm{D}}{3\,\mathrm{MeV}}\right)^{-2/5}, \\ \qquad\qquad \left(1\times10^{12}\,\mathrm{GeV}\lesssim\tilde{f}_a\lesssim 5\times10^{14}\,\mathrm{GeV}\right), \\ 0.22\,\mathrm{GeV}\left(\dfrac{m_{\mathrm{MLSP}}}{100\,\mathrm{GeV}}\right)^{6/5}\left(\dfrac{Y_b}{10^{-10}}\right)^{-2/5}\left(\dfrac{f_a}{10^{14}\,\mathrm{GeV}}\right)^{-2/5}\left(\log\dfrac{f_a}{10^3\,\mathrm{GeV}}\right)^{2/5}\left(\dfrac{T_\mathrm{D}}{3\,\mathrm{MeV}}\right)^{-2/5}, \\ \qquad\qquad \left(5\times10^{14}\,\mathrm{GeV}\lesssim\tilde{f}_a\right). \end{cases} \tag{51}
$$

We show the allowed region for the parameters $m_{\tilde{a}}$ and f_a in both the KSVZ and the DFSZ models in Fig. 2. The lower left region is excluded by the BBN constraints (blue solid line). The upper right region is excluded by the condition $m_{\tilde{a}} < \frac{M_Q}{Q}$ [Eqs.(50) and (51)].

In the KSVZ model (the left panel), the upper left region is excluded by the condition $\epsilon \leq 1$ [See Eqs.(25)], above which we cannot have enough baryon number compared to the axino dark matter. On the other hand, in the DFSZ model (the right panel), the upper left region is excluded by the condition that the higgsino decay produces too much axinos [Eq.(44)], which is the main difference from the KSVZ model and considerably cuts out the allowed region compared with that in the KSVZ case.

In the KSVZ model, the allowed region is bounded from below for both f_a and $m_{\tilde{a}}$. The former is due to the fact that the observed neutrino cooling of SN 1987A excludes the axion decay constant smaller than 6×10^9 GeV [27], shown as the grey hatched regions in Fig. 2. The latter comes from the constraint on the Q-ball parameter M_F such that $M_F \lesssim 0.1\sqrt{m_{3/2}M_\mathrm{P}} = 0.1\sqrt{m_{\tilde{a}}M_\mathrm{P}}$ [see Eq.(1)]. Using Eqs.(27) with $Y_b = 10^{-10}$ and (14), together with Eqs.(37) or (39), we obtain the lower limit of $m_{\tilde{a}}$ as

$$
m_{\tilde{a}} \gtrsim \begin{cases} 0.4\,\mathrm{MeV} & \left(T_{\mathrm{RH,max}}^{(\mathrm{KSVZ}\ \tilde{a})} < T_{\mathrm{RH,max}}^{(3/2)}\right), \\ 3\,\mathrm{MeV}\left(\dfrac{f_a}{10^{10}\,\mathrm{GeV}}\right)^{-5/2}\left(\dfrac{T_\mathrm{D}}{3\,\mathrm{MeV}}\right)^{3/2} & \left(T_{\mathrm{RH,max}}^{(\mathrm{KSVZ}\ \tilde{a})} > T_{\mathrm{RH,max}}^{(3/2)}\right). \end{cases} \tag{52}
$$

This is shown by the dark blue dotted line in the left panel of Fig. 2.

The allowed region is split into four (three) different realizations in the KSVZ (DFSZ) model. The Q-ball decay into axinos is saturated in the left side of the pink long-dashed line, while it is unsaturated in its right side. The orange dotted line divides whether the abundance of thermally produced gravitinos or axinos determines the upper limit of the reheating temperature $T_{\mathrm{RH,max}}$. We also plot $T_{\mathrm{RH,max}}$ contours in green dashed lines, the upper right of which is allowed for certain reheating temperature.

We find that the scenario works for rather wide range in the parameter space such that $6\times10^9\,\mathrm{GeV} \lesssim f_a \lesssim 5\times10^{14}\,\mathrm{GeV}$ and $m_{\tilde{a}} = O(\mathrm{MeV}) - O(\mathrm{GeV})$ in the KSVZ model, while the allowed region is restricted to $f_a \gtrsim 10^{12}\,\mathrm{GeV}$ in the DFSZ model.

5.4 Realizations of the successful scenario in the Q-ball parameters

We find above the allowed region in the parameter space (f_a, $m_{\tilde{a}}$). Here we show the realizations of the successful scenario for particular parameter sets of (f_a, $m_{\tilde{a}}$) in terms of Q-ball parameters, Q and M_F.

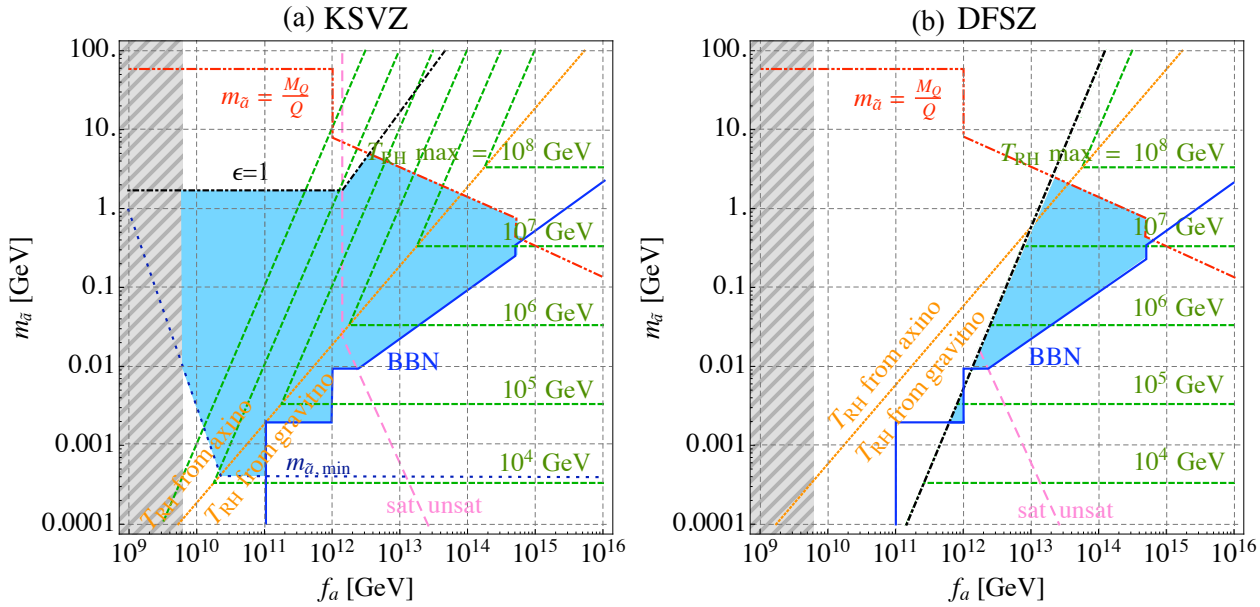

Figure 2: Allowed regions in (f_a, $m_{\tilde{a}}$) plane for the KSVZ (left) and the DFSZ (right) models are shown as blue filled regions. In both panels, above the blue solid lines, the lower limit of the MLSP abundance satisfies the BBN constraint [see fig. 1]. Below the red dashed double-dotted lines, Q balls can decay into axinos [Eqs.(50) and (51)]. The grey hatched regions are excluded by the SN1987 observation. In the left panel (KSVZ case), the black dashed dotted line denotes $\epsilon = 1$, below which the simultaneous explanation of the dark matter and the baryon asymmetry is achievable [see Eq.(25)], and the dark blue dotted line is the lower bound Eq.(52). The black dashed dotted line in the right panel (the DFSZ case) represents Eq.(44), above which the axinos are overproduced by the higgsino decay. The pink long-dashed lines divide the Q-ball decay into the saturated (on their left side) and unsaturated (on their right side) cases. The orange short-dashed lines distinguish which the upper limit of $T_{\rm RH}$ comes from: the thermally produced axinos (their above) or gravitinos (their below). The green dashed lines denote the iso-$T_{\rm RH,max}$ contours.

In the first place, Q is expressed by the MLSP abundance. Using Eq.(30) for the saturated case, and Eq.(31) for the unsaturated case, we respectively obtain the relation of Q and M_F as

$$Q_{\rm sat} \simeq 6.1 \times 10^3 \left(\frac{\rho_{\rm MLSP}/s}{\rm GeV}\right)^{-1} \left(\frac{m_{\tilde{a}}}{\rm GeV}\right)^{-1} \left(\frac{m_{\rm MLSP}}{100\,\rm GeV}\right)^{-3} \left(\frac{M_{\rm F}}{10^4\,\rm GeV}\right)^{4}, \tag{53}$$

$$\begin{aligned} Q_{\rm unsat} \simeq\ & 5.5 \times 10^{11} \left(\frac{\rho_{\rm MLSP}/s}{\rm GeV}\right)^{-2/3} \left(\frac{m_{\tilde{a}}}{\rm GeV}\right)^{-2/3} \\ & \times \left(\frac{f_a}{10^{14}\,\rm GeV}\right)^{2/3} \left(\log \frac{f_a}{10^3\,\rm GeV}\right)^{-2/3} \left(\frac{m_{\rm MLSP}}{100\,\rm GeV}\right)^{-2} \left(\frac{M_{\rm F}}{10^4\,\rm GeV}\right)^{8/3}. \end{aligned} \tag{54}$$

In the same manner, from Eqs.(27) and (28), we obtain the charge Q in terms of the reheating temperature $T_{\rm RH}$ for the saturated and unsaturated cases as

$$Q_{\rm sat} \simeq 7.1 \times 10^{17} \left(\frac{m_{\tilde{a}}}{\rm GeV}\right)^{-4/3} \left(\frac{\beta}{6 \times 10^{-5}}\right) \left(\frac{T_{\rm RH}}{10^7\,\rm GeV}\right)^{-4/3} \left(\frac{M_F}{10^4\,\rm GeV}\right)^{-4/3}, \tag{55}$$

$$Q_{\rm unsat} \simeq 5.8\times10^{21}\left(\frac{m_{\tilde a}}{\rm GeV}\right)^{-4/5}\left(\frac{f_a}{10^{14}\,\rm GeV}\right)^{4/5}\left(\log\frac{f_a}{10^{3}\,\rm GeV}\right)^{-4/5} \times\left(\frac{\beta}{6\times10^{-5}}\right)^{3/5}\left(\frac{T_{\rm RH}}{10^{7}\,\rm GeV}\right)^{-4/5}\left(\frac{M_F}{10^{4}\,\rm GeV}\right)^{-4/5}, \quad (56)$$

respectively. $T_{\rm D}$-dependence of Q is obtained from Eq.(15) as

$$Q \simeq 1.8\times10^{21}\left(\frac{T_{\rm D}}{3\,\rm MeV}\right)^{-8/5}\left(\frac{M_F}{10^{4}\,\rm GeV}\right)^{4/5}. \quad (57)$$

For each fixed $m_{\tilde a}$ and f_a pair, the allowed region is between the line (53) or (54) with the largest and smallest possibile MLSP abundances, above the line (55) or (56) with the largest possible reheating temperature, and below the line (57). These lines are shown respectively as green dashed, blue solid, and red dashed double-dotted lines in Fig.3 for $f_a = 10^{12} - 10^{14}\,\rm GeV$ and $m_{\tilde a} = 3\,\rm MeV - 3\,GeV$. Also shown is the condition that $bm_N \lesssim M_Q/Q \lesssim m_{\rm MLSP}$, which corresponds to the region between lines

$$Q \simeq 1.2\times10^{19}\left(\frac{M_F}{10^{4}\,\rm GeV}\right)^{4}\left(\frac{M_Q/Q}{\rm GeV}\right)^{-4}, \quad (58)$$

with $M_Q/Q = bm_N$ and $M_Q/Q = m_{\rm MLSP}$, represented by orange short-dashed lines. The other orange short-dashed line corresponds to $M_Q/Q = m_{\tilde a}$.

The filled regions are the allowed parameter space: the dark region applies to the KSVZ model for all the figures, while those regions in $(f_a, m_{\tilde a}) = (10^{12}\,\rm GeV,\ 3\,MeV)$, $(10^{13}\,\rm GeV,\ 30\,MeV)$, $(10^{14}\,\rm GeV,\ 300\,MeV)$, and the dark and light regions in $(10^{13}\,\rm GeV,\ 300\,MeV)$ correspond to the DFSZ case. We see that our scenario works typically for $Q = 10^{20} - 10^{22}$ and $M_F = 10^4 - 10^6$ GeV.

6 Summary

We have investigated the Q-ball scenario in the gauge-mediated SUSY breaking model where the Q ball decays into axinos and nucleons, providing simultaneously the dark matter and the baryon asymmetry of the universe. The branching of the Q-ball decay into axinos is typically small, but the decay would be saturated for small f_a region. This is in contrast to the branching into the gravitino, where it is always much smaller compared to the decay into axinos, so that we could safely neglect any effects of the gravitino on our scenario.

In our scenario, the Q ball has small enough charge to decay into nucleons and axinos, while it is large enough to kinematically forbid the decay channel to the SUSY particles in the MSSM, e.g., the lightest neutralinos. This prohibition holds almost through the decay process until the very end of the decay when the charge becomes small enough to open the channel into the MSSM LSPs, or MLSPs. We have evaluated the MLSP abundance, and imposed the condition that it should not affect the success of the BBN, which has resulted in the upper limit on the MLSP abundance. Meanwhile, the lower bound of the MLSP abundance has been obtained by the highest possible reheating temperature which comes from the condition that the thermally produced axinos and/or gravitinos are not the dominant component of the dark matter of the universe.

These conditions have led us to constrain the axino model parameters, the axino mass $m_{\tilde a}$ and the axion decay constant f_a, as well as from the condition that the axino can be produced kinematically from the Q-ball decay. The successful scenario resides in the region typically where $m_{\tilde a} = O(\rm MeV) - O(\rm GeV)$ and $6\times10^9\,\rm GeV \lesssim f_a \lesssim 5\times10^{14}\,\rm GeV$ in the KSVZ model, while the small f_a region ($f_a \lesssim 10^{12}\,\rm GeV$) is excluded in the DFSZ model.

We also have seen the realization of the successful scenario in terms of the Q-ball parameters, Q and M_F. The typical parameters are $Q = 10^{20} - 10^{22}$ and $M_F = 10^4 - 10^6\,\rm GeV$.

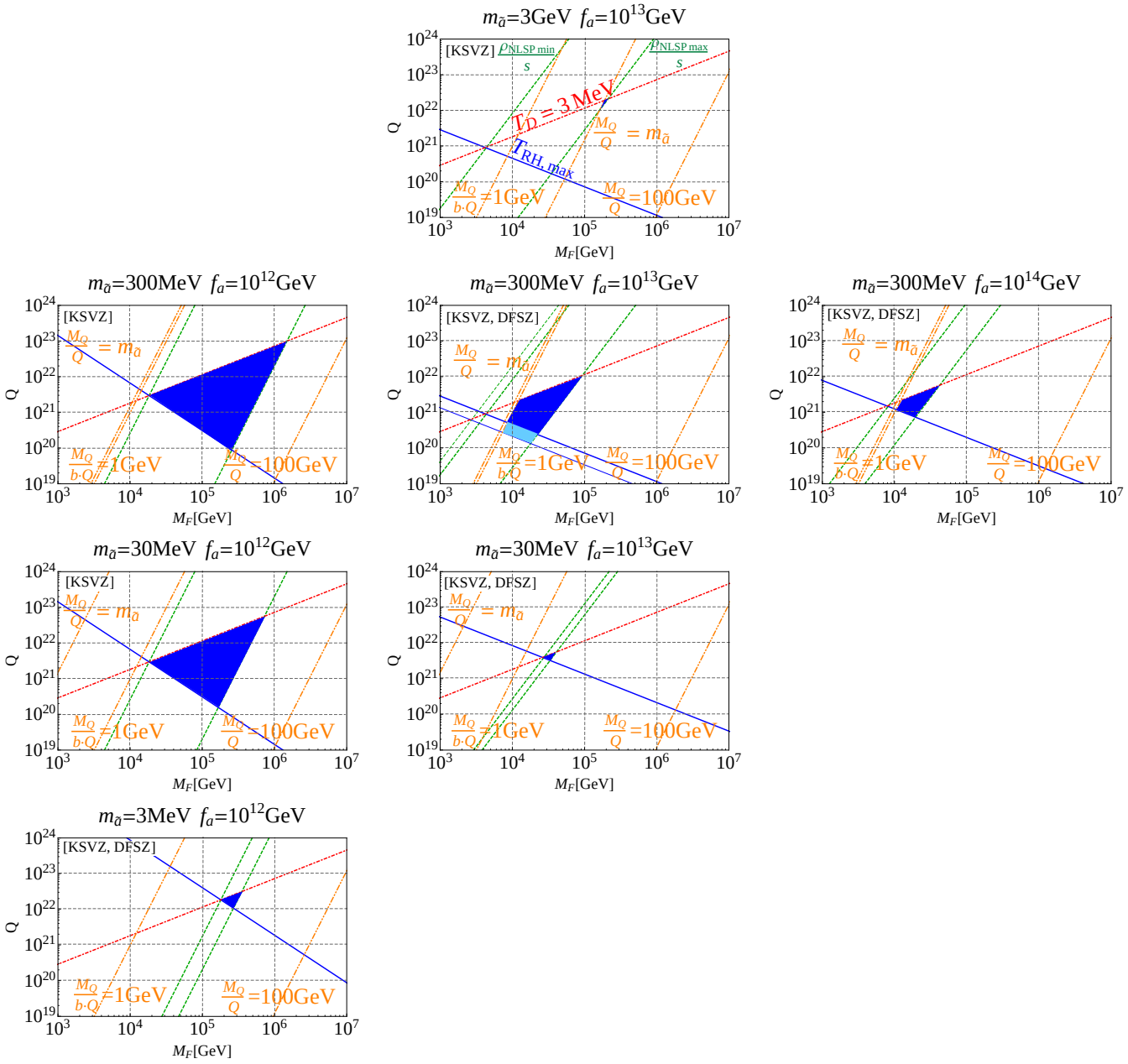

Figure 3: Allowed region for the Q-ball parameters $M_{\rm F}$ and Q for the KSVZ and DFSZ as indicated in the figures. It is shown for $f_a = 10^{12}$, 10^{13}, and $10^{14}\,$GeV from the left column to the right, respectively, and $m_{\tilde{a}} = 3$, 30, 300 MeV, and 3 GeV from the bottom row to the top, respectively. Blue solid lines show Eq.(55) or Eq.(56) with the largest possible $T_{\rm RH}$ from the constraint of the axino/gravitino thermal production. Upper and lower green dashed lines show Eq.(53) or Eq.(54) with the minimum and maximum MLSP abundances, respectively (see Fig. 1). Thin blue solid and thin green dashed lines apply to the DFSZ model for $m_{\tilde{a}} = 300\,$MeV and $f_a = 10^{13}\,$GeV case. Red dashed dotted lines represents Eq.(57) with $T_{\rm D} = 3\,$MeV, below which is allowed. Orange dashed double-dotted lines denote Eq.(58) with $\frac{M_Q}{Q} = m_{\rm MLSP}$, $\frac{M_Q}{bQ} = m_N$, and $\frac{M_Q}{Q} = m_{\tilde{a}}$ (where shown) from the right to the left, respectively, exception being for $m_{\tilde{a}} = 3\,$GeV case, as shown in the figure.

Finally, we comment on the free streaming of the axinos. Because of the rather large kinetic energy of the axinos emitted from Q balls, the free streaming might affect the structure formation of the universe. For the parameters for the successful scenario, we have shorter free streaming length than $\sim$ Mpc. Thus, we can safely neglect such effects.

Acknowledgments

The work is supported by Grant-in-Aid for Scientific Research 23740206 (S.K.), 14102004 (M.K.) and 21111006 (M.K.) from the Ministry of Education, Culture, Sports, Science and Technology in Japan, and also by World Premier International Research Center Initiative (WPI Initiative), MEXT, Japan.

A Axino productions in SUSY axion models

Here we briefly explain how the axinos are produced in the SUSY axion models. We are mainly interested in the nonthermal axino production from the Q-ball decay, which accounts for the dark matter of the universe in our scenario. We also show the thermally produced axinos from the scatterings and the higgsino decay, whose abundance must not be the main component of the dark matter. In addition, we see the decay of the MLSP into the axino, used for the BBN constraint.

Let us start from the two classes of axion models, the KSVZ [28] and the DFSZ [29] models in the context of SUSY [30, 31]. In both cases, the superpotential responsible for the spontaneous PQ symmetry breaking is written as [32]

$$W_{\rm PQ} = f_Z Z \left(S_1 S_2 - V_a^2 \right), \tag{A.1}$$

where Z, S_1, and S_2 are gauge singlet chiral superfields, f_Z is a coupling and V_a is a VEV for S_1 and S_2. In KSVZ model, they introduced new heavy quarks which carry PQ charges. The superpotential is written as [28]

$$W_{\rm KSVZ} = W_{\rm PQ} + f_Q Q_L \bar{Q}_R S_1. \tag{A.2}$$

The second term leads to the anomaly coupling $aG\tilde{G}$ at low energy after the heavy quarks are integrated out. On the other hand, in DFSZ model, two Higgs doublets, H_d and H_u, and MSSM (s)quarks, carry PQ charges and couples to the axion multiplet as [31]

$$W_{\rm DFSZ} = W_{\rm PQ} + \frac{f_s}{M_{\rm P}} S_1^2 H_d H_u. \tag{A.3}$$

The anomalous coupling is obtained after electroweak symmetry breaking through the coupling of the axion to the higgs doublets which further couples to the light (s)quarks.

The elementary process of the Q-ball decay into axino is squark $\to$ quark + axino. The dominant part of the coupling comes from the logarithmically divergent part of the gluon-gluino-(s)quark loop term. The effective coupling is given by [19]

$$f_{\rm eff}^{(\tilde{a})} = \frac{\alpha_s^2}{\sqrt{2}\pi^2} \frac{m_{\tilde{g}}}{f_a} \log\left(\frac{f_a}{m_{\tilde{g}}} \right). \tag{A.4}$$

In the DFSZ model, there also exists a tree-level axino-quark-squark coupling, but the rate is proportional to (quark mass)^2 [26], which is negligible in our scenario.

Next we want to estimate the abundance of the axinos thermally produced by scattering processes. In this paper, we adopt the results of Ref.[24]. We notice that it is only valid for small coupling regime, and there may be ambiguities of about an order of the magnitude [24, 33, 26], or even some controversies on the estimate of the axino-gluon-gluino coupling [34].

The axino production from the scattering via the axino-gluino-gluon interaction can be expressed in a gauge invariant way. The axino yield, $Y_{\tilde{a}} = \frac{n_{\tilde{a}}}{s}$, at present can be obtained by

$$Y_{\tilde{a}} \simeq \frac{C_{\tilde{a}}(T_{\rm RH})}{s(T_{\rm RH})H(T_{\rm RH})}, \tag{A.5}$$

with the collision term for SU(N) [24]

$$C_{\tilde{a}}(T) \simeq \frac{(N^2-1)}{f_a^2}\frac{3\zeta(3)g^6T^6}{4096\pi^7}\left[\log\left(\frac{1.647T^2}{m_g^2}\right)(N+n_f)+0.4336n_f\right], \tag{A.6}$$

where g is a coupling constant of SU(N) and n_f is a number of SU(N) multiplet and anti-multiplet, and $m_g = gT\sqrt{\frac{N+n_f}{6}}$ is the thermal SU(N)-gaugino mass. Here, we use the Hubble parameter $H(T) = \sqrt{\frac{g_*(T)\pi^2}{90}}\frac{T^2}{M_{\rm P}}$ and the entropy density $s(T) = \frac{2\pi^2}{45}g_*(T)T^3$, where g_* is the number of effectively massless degrees of freedom and we use $g_* = 228.75$. Then the axino density parameter is estimated as

$$\begin{aligned}\Omega_{\tilde{a}}^{\rm TH}h^2 &= m_{\tilde{a}}Y_{\tilde{a}}\frac{s(T_0)h^2}{\rho_c},\\ &\simeq 7.7\times10^{-4}g^6(N^2-1)\left(\frac{m_{\tilde{a}}}{\rm GeV}\right)\left(\frac{f_a}{10^{14}\,\rm GeV}\right)^{-2}\left(\frac{T_{\rm RH}}{10^7\,\rm GeV}\right)\\ &\quad\times\left[\log\left(\frac{3.144}{g\sqrt{N+n_f}}\right)(N+n_f)+0.2168n_f\right],\end{aligned} \tag{A.7}$$

where ρ_c is the present critical density.

When the SU(3) anomaly term is present as in the KSVZ model, Eq.(A.7) can be rewritten as

$$\Omega_{\tilde{a}}^{\rm TH(KSVZ)}h^2 = 1.0\times10^{-2}\left(\frac{m_{\tilde{a}}}{\rm GeV}\right)\left(\frac{f_a}{10^{14}\,\rm GeV}\right)^{-2}\left(\frac{T_{\rm RH}}{10^7\,\rm GeV}\right), \tag{A.8}$$

where g is the coupling constant of SU$(3)_C$, and we use $g = 0.983$, the value at 10^6 GeV, and $n_f = 6$ in the second equality. When the SU(3) anomaly term is absent as in the case for high temperature regime in the DFSZ model, we need to consider the SU$(2)_L$ anomaly term [26]. Eq.(A.7) is then given as

$$\Omega_{\tilde{a}}^{\rm TH(DFSZ)}h^2 = 1.1\times10^{-3}\left(\frac{m_{\tilde{a}}}{\rm GeV}\right)\left(\frac{f_a}{10^{14}\,\rm GeV}\right)^{-2}\left(\frac{T_{\rm RH}}{10^7\,\rm GeV}\right), \tag{A.9}$$

where $N = 2$, $n_f = 14$ and $g = 0.663$, estimated at 10^6 GeV, are used.

In the DFSZ model, there also exists a tree-level axino-higgs-higgsino coupling which contributes to the thermally production of axinos by the higgsino decay whose decay rate is given by [25, 26]

$$\Gamma_{\tilde{h}} \simeq c_H^2\left(\frac{\mu}{f_a}\right)^2\frac{m_{\tilde{h}}}{16\pi}, \tag{A.10}$$

where $c_H^2 = 8$. We take the higssino mass $m_{\tilde{h}} = \mu = 200$ GeV. The yield of axino from the higgsino decay is estimated as $Y_{\tilde{a}}^{(\tilde{h})} \simeq 5\times10^{-4}g_{\tilde{h}}M_{\rm P}\Gamma_{\tilde{h}}/m_{\tilde{h}}^2$, where $g_{\tilde{h}} = 2$ is the higgsino degrees of freedom [35]. Then, the axino production from this decay is dominant at the low reheating temperature, $T_{\rm RH} \lesssim 2\times10^7$ GeV, and the density of the axino is given by [25, 26]

$$\Omega_{\tilde{a}}^{\rm TH(\tilde{h})}h^2 = 2.0\times10^{-3}\left(\frac{m_{\tilde{a}}}{\rm GeV}\right)\left(\frac{f_a}{10^{14}\,\rm GeV}\right)^{-2}. \tag{A.11}$$

Finally, we evaluate the MLSP decay into axinos. Here we consider the neutralino as the MLSP, then the decay rate is given by [35]

$$\begin{aligned}\Gamma_{\rm MLSP} &= \frac{\alpha_{\rm em}^2 C^2}{128\pi^3}\frac{m_{\rm MLSP}^3}{f_a^2}\left(1-\frac{m_{\tilde{a}}^2}{m_{\rm MLSP}^2}\right)^3, \\ &\simeq 1.3\times 10^{-30}\,{\rm GeV}\left(\frac{f_a}{10^{14}\,{\rm GeV}}\right)^{-2}\left(\frac{m_{\rm MLSP}}{100\,{\rm GeV}}\right)^3, \end{aligned} \tag{A.12}$$

where $\alpha_{\rm em} = 1/137$ is the electromagnetic coupling strength and C is a model dependent parameter which we take $C = 1$. In our scenario, the MLPS production is kinematically forbidden until the very end of the Q-ball decay, but its abundance is severely constrained by the BBN.

References

[1] I. Affleck and M. Dine, Nucl. Phys. B **249**, 361 (1985).

[2] A. Kusenko and M. E. Shaposhnikov, Phys. Lett. B **418**, 46 (1998).

[3] K. Enqvist and J. McDonald, Phys. Lett. B **425**, 309 (1998); Nucl. Phys. **B538**, 321 (1999); Phys. Lett. **B440**, 59 (1998).

[4] S. Kasuya and M. Kawasaki, Phys. Rev. D **61**, 041301(R) (2000).

[5] S. Kasuya and M. Kawasaki, Phys. Rev. D **62**, 023512 (2000).

[6] S. Kasuya and M. Kawasaki, Phys. Rev. D **64**, 123515 (2001).

[7] M. Fujii, K. Hamaguchi, Phys. Lett. **B525**, 143 (2002).

[8] O. Seto, Phys. Rev. **D73**, 043509 (2006).

[9] L. Roszkowski and O. Seto, Phys. Rev. Lett. **98**, 161304 (2007)

[10] I. M. Shoemaker and A. Kusenko, Phys. Rev. D **80**, 075021 (2009).

[11] F. Doddato and J. McDonald, JCAP **1106**, 008 (2011).

[12] S. Kasuya and M. Kawasaki, Phys. Rev. D **84**, 123528 (2011).

[13] R. D. Peccei and H. R. Quinn, Phys. Rev. Lett. **38**, 1440 (1977).

[14] S. Kasuya and F. Takahashi, JCAP **0711**, 019 (2007).

[15] A. de Gouvêa, T. Moroi and H. Murayama, Phys. Rev. D **56**, 1281 (1997).

[16] A. G. Cohen, S. R. Coleman, H. Georgi and A. Manohar, Nucl. Phys. B **272**, 301 (1986).

[17] J. R. Ellis, J. S. Hagelin, D. V. Nanopoulos, K. A. Olive and M. Srednicki, Nucl. Phys. B **238**, 453 (1984).

[18] K. Nakamura *et al.* [Particle Data Group], J. Phys. G **37**, 075021 (2010).

[19] L. Covi, L. Roszkowski and M. Small, JHEP **0207**, 023 (2002).

[20] N. Jarosik *et al.*, Astrophys. J. Suppl. **192**, 14 (2011).

[21] M. Kawasaki, K. Kohri and T. Moroi, Phys. Rev. D **71**, 083502 (2005); K. Kohri, T. Moroi and A. Yotsuyanagi, Phys. Rev. D **73**, 123511 (2006); M. Kawasaki, K. Kohri, T. Moroi and A. Yotsuyanagi, Phys. Rev. D **78**, 065011 (2008).

[22] M. Kawasaki, F. Takahashi and T. T. Yanagida, Phys. Rev. D **74**, 043519 (2006).

[23] E. J. Chun, J. E. Kim and H. P. Nilles, Phys. Lett. B **287**, 123 (1992); E. J. Chun and A. Lukas, Phys. Lett. B **357**, 43 (1995); P. Moxhay and K. Yamamoto, Phys. Lett. B **151**, 363 (1985); T. Goto and M. Yamaguchi, Phys. Lett. B **276**, 103 (1992).

[24] A. Brandenburg and F. D. Steffen, JCAP **0408**, 008 (2004).

[25] E. J. Chun, Phys. Rev. D **84**, 043509 (2011).

[26] K. Y. Choi, L. Covi, J. E. Kim and L. Roszkowski, arXiv:1108.2282 [hep-ph].

[27] E. W. Kolb and M. S. Turner, *The Early Universe* (Addison-Wesley, Reading, MA, 1990).

[28] J. E. Kim, Phys. Rev. Lett. **43**, 103 (1979); M. A. Shifman, A. I. Vainshtein and V. I. Zakharov, Nucl. Phys. B **166**, 493 (1980).

[29] M. Dine, W. Fischler and M. Srednicki, Phys. Lett. B **104**, 199 (1981); A. R. Zhitnitsky, Sov. J. Nucl. Phys. **31**, 260 (1980) [Yad. Fiz. **31**, 497 (1980)].

[30] H. P. Nilles and S. Raby, Nucl. Phys. B **198**, 102 (1982).

[31] J. E. Kim and H. P. Nilles, Phys. Lett. B **138**, 150 (1984).

[32] J. E. Kim, Phys. Lett. B **136**, 378 (1984).

[33] A. Strumia, JHEP **1006**, 036 (2010).

[34] K. J. Bae, K. Choi and S. H. Im, JHEP **1108**, 065 (2011).

[35] L. Covi, H. -B. Kim, J. E. Kim and L. Roszkowski, JHEP **0105**, 033 (2001).